Effect of salinity on solution properties of a partially hydrolyzed polyacrylamide

Zsófia Vargáné Árok [a], Szilárd Sáringer [a], Dóra Takács [a], Coline Bretz [b], Ádám Juhász [a,c,*], Istvan Szilagyi [a,*]

[a] MTA-SZTE Lendület Biocolloids Research Group, Interdisciplinary Excellence Center, Department of Physical Chemistry and Materials Science, University of Szeged, H-6720 Szeged, Hungary
[b] LS Instruments AG, CH-1700 Fribourg, Switzerland
[c] MTA-SZTE Lendület "Momentum" Noble Metal Nanostructures Research Group, University of Szeged, H-6720 Szeged, Hungary

ABSTRACT

The growing energy demand requires maximization of oil recovery from known reserves, while enhanced oil recovery (EOR) techniques are focused on sweeping residuals available in reservoirs previously flooded with water. Polymer additives are widely applied in EOR processes, as they can increase the viscosity and reduce the water permeability leading to mobility decrease of the injected solution. In this study, structural and rheological characterizations of a partially hydrolyzed polyacrylamide (FLOPAAM 3630S) were performed in a wide range of salinity relevant to conditions in existing oil reservoirs. Macromolecular solutions were identified at low polymer concentrations and/or at elevated salt levels, while gelation, i.e., formation of coherent structure, was observed at high FLOPAAM 3630S doses at low salinity. The transition points between these stages were determined and a comparison of scattering and rheology measurements revealed that the driving force of such a transformation is of non-electrostatic origin, but rather relies on the hydrophobic intermolecular interactions. The results bring new insights into the design of efficient EOR processes applied in oil reservoirs of different salt levels.

1. Introduction

Polymers are widely used in the oil production industry [1–4]. Accordingly, they are applied in near-well treatments to expand the performance of water injectors by blocking off high-permeability zones [5], as reactants to be cross-linked in situ to plug high conductivity zones at depth in the reservoir [6] and as additives to reach lower water–oil mobility ratio [7]. The latter function of the polymers in the oilfield chemical industry is exploited in polymer flooding processes, which is one of the most profitable and extensively applied chemical enhanced oil recovery (EOR) techniques [8]. Furthermore, conventional EOR processes include chemical flooding, gas injection and thermal recovery. These methods involve the addition of the displacing substance into the reservoir through the injection well to displace the remaining oil, and such substances are usually aqueous solutions of surfactants and polymers in chemical flooding [2,9,10]. The recovery of oil from subsurface reservoirs frequently requires the injection of water to improve oil sweep and maintain the reservoir pressure. Based on the most assumed

reservoir model, the lifetime of a hydrocarbon reservoir is commonly divided into three main stages. While in the primary period, the recovery occurs via naturally driven oil extraction mechanisms, in the secondary phase, the recovery is carried out by techniques used to maintain the reservoir pressure through water or gas injection. EOR is typically applied for oil reservoirs, once secondary recovery operations have been carried out, as the third stage [11].

In a pioneering study by Sandiford [12], polymer flooding has been recommended as an EOR procedure to improve the viscosity of the displacing fluid. This discovery was followed by extensive research attempts with the objective to apply non-Newtonian displacing fluids in EOR [13,14]. Frequently, the mobility ratio between displacing medium and displaced oil is unfavourably large, which results in a significant amount of bypassed oil. Therefore, instead of pure water or surfactant solution, the polymer was added to injection water to enhance water-flooding sweep efficiency by increasing the viscosity of the injected fluid and reducing its mobility. While polymer flooding is a relatively well-studied and widely discussed method in the literature [4,8,15,16], the

mechanism, and phenomena of polymer flow in a porous medium are not yet completely understood [17]. The challenges in understanding polymer flow in porous media arise from the intricate interactions between the polymer solution and the porous structure. Factors such as molecular weight, concentration, and viscosity of the polymer, as well as the porosity and permeability of the media, affect the flow behavior. In addition, possible polymer adsorption on porous surfaces, shear-thinning or thickening, and viscoelastic effects further complicate the interpretation [18].

Another phenomenon that has been much discussed but not yet elucidated is immiscible viscous fingering, and accurate modelling, which is essential in understanding the fluid distribution in the reservoirs [19]. This manifestation of propagating chemical patterns can be detected by injecting another fluid of lower viscosity, immiscible, into a viscous liquid. The loss of interface stability results in the formation of finger-like shapes, unstable fronts, or detached fluid islands [20]. The phenomenon was first studied and noted by Hill [21], and then Taylor and Saffman explored the arrangement, in which a higher viscosity fluid is located above a lower viscosity fluid in a water–oil and glycerin-oil system from both experimental and theoretical points of view [22]. When examining the deformation of a surface due to a difference in viscosity, it has been found that there is a critical value for the wavelength of the resulting pattern and at smaller values, the surface tension is still able to stabilize the shape of the pattern. Numerical simulations provide an opportunity for theoretical modelling of the patterns resulting from viscosity change [23], which is being integrated into reservoir engineering tasks. Therefore, it can be concluded that the most detailed physicochemical characterization of the fluid to be injected during polymer flooding can help to run more accurate numerical simulations and thus, to design the correct fluid technology plan. Among the first attempts for simulation of viscous fingering in porous media, in the pioneering work of Peaceman and Rachford [24], partial differential equations illustrating miscible displacement of fluids in porous media were derived.

The salinity of water present in oil reservoirs is another important challenge to tackle during polymer flooding [25,26]. Accordingly, optimization of the flow behavior of polymer solutions in heavy oil tanks in the presence of electrolytes, whose concentration can be extremely high, is challenging due to the lack of comprehensive experimental data on the viscoelastic properties of polymers recorded at relevant conditions [27]. Moreover, the EOR efficiency of the displacing medium is highly dependent on the colloidal stability of the surfactant-polymer systems, which is sensitive to the solution environment such as pH, temperature, and salinity. Therefore, the oil industry has shown great interest in the maintenance of ideal polymer selection and stability in a wide range of total dissolved solids [28–30]. Salinity also influences the non-Newtonian shear-dependent in-situ rheology of polymer solutions through the impact on polymer injectivity under reservoir conditions. The main challenge that faces prognostication of polymer injectivity in field applications is the non-Newtonian characteristics of polymer solutions [17,26], which may indicate complex behavior including shear-thickening at high flow rates in addition to the typical shear-thinning character at low rates. Precise and detailed modelling of these phenomena is crucial to perform, as it provides a deeper understanding of fluid distribution in the reservoir before polymer flooding.

Therefore, in the present paper, the solution characteristics of a FLOPAAM 3630S polymer were systematically investigated by rheology and light scattering techniques in a wide range of polymer concentrations and salinity. FLOPAAM is a series of partially hydrolyzed polyacrylamides along with SUPERPUSHER and FLOCOMB, which are water-soluble co– and ter-polymers frequently used in EOR flooding applications. The advantages of applying FLOPAAM polymers include their low cost and high molecular weight [31]. The polyacrylamide derivate used in this study is a commercially available liquid thickener and its salinity-dependent viscoelastic properties were not studied in the past in detail. The present results contribute to the design of an improved polymer solution composition under the desired EOR conditions.

2. Experimental

2.1. Materials

Partially hydrolyzed polyacrylamide (FLOPAAM 3630S, SNF Floerger) was received from MOL Plc and NaCl was purchased from VWR (Debrecen, Hungary). For FLOPAAM 3630S, the manufacturer reported an average molecular mass of 2×10^7 g/mol and 30% anionic charge. All reagents were used without further purification. Ultrapure water was produced with a VWR Puranity TU + device for all sample preparations. Salt solutions were filtered with a 0.1 mm PVDF syringe filter purchased from Millex (Budapest, Hungary). The measurements were performed at (25.0 ± 0.1) °C.

2.2. Methods

2.2.1. Preparation of polymer solutions

A stock FLOPAAM 3630S solution (500 mL) was prepared at a concentration of 5 g/L by dissolving the solid polymer samples in the water while stirring for at least 12 h under a nitrogen atmosphere. To prepare the samples containing electrolytes, the calculated mass of solid NaCl was placed in a 100 mL volumetric flask and then, ultrapure water was added to the crystalline material until complete dissolution. Thereafter, 20 mL of polymer stock solution was added using a plunger glass pipette. The volumetric flask was then filled with ultrapure water and the solution was stirred for at least 12 h to homogenize the sample.

2.2.2. Rheological investigation of polymer samples

The shear and oscillatory rheology measurements were carried out via a stress-controlled rheometer (MCR 302, Anton Paar) fitted with double gap, concentric cylinder geometry (CC27-SN12793) and pressure cell [32]. Controlled shear stress tests were conducted by varying the shear rate. Rheological studies are carried out at six different conditions of ionic strength (from 0.462 to 4620 mM adjusted with NaCl) at constant temperature (25 °C) and atmospheric pressure. After loading, the samples were held for 5 min at the test temperature before measurements to allow stress relaxation and temperature equilibration. During the rotational tests, a range of shear rate ($\dot{\gamma}$) from 1 to 1000 s^{-1} was applied, while shear stress (τ) and apparent viscosity (η) were recorded at different $\dot{\gamma}$ values. The data were collected by Anton Paar Rheo-Compass software. The primary experimental data from the flow curves were analyzed using the Herschel-Bulkley model [33]:

$$\tau = \tau_0 + k\dot{\gamma}^n \tag{1}$$

where τ_0 is the yield point, which gives the minimum shear required for the liquid to flow, n is the flow index and k is the consistency index or apparent viscosity that characterizes the resistance of the system against the flow. In the case of a Newtonian fluid, the value of n is near to unity, τ_0 can be determined from the intersection of the extrapolated linear region of the flow curves and k can be derived from the slope of this linear section. When $n < 1$, the Herschel-Bulkley fluid behaves as shear-thinning, whereas if $n > 1$, as shear-thickening material. In addition to the Bingham model [34], the Carreau-Yasuda equation [35] was used to fit the viscosity curves for the shear-thinning polymer solutions:

$$\eta = \eta_\infty + (\eta_0 - \eta_\infty)[1 + (\lambda\dot{\gamma})^a]^{(n-1)/a} \tag{2}$$

This model contains five adjustable parameters ($a, \eta_0, \eta_\infty, \lambda, n$) to fit the model to experimental data (η as a function of $\dot{\gamma}$). At low shear rates in polymeric systems (both melts and solutions), the apparent viscosity approaches a Newtonian plateau, where η is independent of $\dot{\gamma}$, referred to as zero-shear viscosity (η_0). Furthermore, polymer solutions also exhibit a similar plateau at very high $\dot{\gamma}$ values leading to the so-called infinite

shear viscosity (η_∞). The relaxation time (λ) is the time associated with large-scale microscopic motions in the structure of the polymer. Besides these parameters, the Carreau-Yasuda model contains two constants, namely, the power-law index, where $n < 1$ that characterizes the degree of shear-thinning of the model and the constant a that sets the size and curvature of the crossover region between the Newtonian and shear-thinning behavior.

The gel-like samples were subjected to periodic oscillation in amplitude frequency sweep tests to evaluate the dependence of the viscoelastic parameters, such as the elastic and viscous moduli, upon a change in the frequency. In dynamic measurements, the sample is subjected to a sinusoidal shear strain (γ) as:

$$\gamma = \gamma_0 \sin(\omega t) \tag{3}$$

where γ_0 is the shear strain amplitude, ω is the oscillation frequency, which can be also expressed as 2π multiplied by the frequency in Hz, and t is the time. The mechanical response, expressed as τ of the viscoelastic materials, is intermediate between an ideal elastic solid (obeying Hooke's law) and an ideal viscous fluid (obeying Newton's law) and therefore, it is out of phase concerning the imposed deformation as expressed by:

$$\tau = G'(\omega)\gamma_0\sin(\omega t) + G''(\omega)\gamma_0\cos(\omega t) \tag{4}$$

where G' is the shear storage modulus or elastic modulus, and G'' is the shear loss modulus or viscous modulus. The elastic modulus describes the capability of the sample to return to the initial configuration after the deformation. The ratio between these moduli is expressed by the loss factor (tanδ) as [35]:

$$\tan\delta = \frac{G''}{G'} \tag{5}$$

where δ is the phase angle, which is equal to 90° for an ideal viscous fluid, 0° for an ideal elastic material, and $0^0 < \delta < 90^0$ for viscoelastic materials. Dynamic viscoelastic measurements of the hydrogel samples were carried out with a strain sweep (0.01–100%) at a fixed frequency of 10 Hz. The G' and G'' as a function of γ were continuously determined during the test. Based on the shape of these functions the flow point (τ_{fp}) and cross-over point ($\dot{\gamma}_{cop}$) of the viscoelastic fluids were evaluated by the above-mentioned rheological software.

Primary experimental and fitted data from rotational and oscillatory measurements are presented in the Supplementary data (SD) in Table S1, Fig. S1 and Fig. S2.

2.2.3. 3D cross-correlation light scattering measurements

The basis of dynamic light scattering (DLS) experiments for nano-sized objects is based on the Brownian motion and the scattered intensity is plotted as a function of time and the autocorrelation function is analyzed to determine diffusion coefficient and to relate their values to hydrodynamic diameter via the Stokes-Einstein equation [36,37]. While in a conventional DLS test, multi-scattering events can sharply affect the results, a 3D cross-correlation experiment eliminates multiple scattering during the measurement and considers individual single scattering events [38]. This can be implemented by using two laser beams that impact the analyzed spot and two high-speed detectors. Thereby, translucent, and turbid samples can be measured even at a high concentration of dispersed material and the need for dilution tests to obtain reliable results is drastically lowered. Based on this practical solution, time-dependent behavior, such as particle–particle interactions or growth of agglomerates can directly be observed at high concentrations of the scattering objects.

For 3D DLS in the present work, the measurements were performed on a LS spectrometer (LS Instruments) that implements the 3D cross–correlation technology, mentioned above. The device is equipped with a 660 nm Cobolt laser with a maximum power of 100 mW and two detectors. The scattering angle was set to 90° and the data were recorded

at 20 °C. Data analysis was performed using the CORENN algorithm (LS Instruments).

2.2.4. Electrophoretic light scattering measurements

The electrophoretic light scattering measurements were performed on a Litesizer 500 device (Anton Paar) using a 40 mW semiconductor laser operating at a 658 nm wavelength. The samples for this type of light scattering measurements were prepared in the same way as detailed in chapter 2.2.1. The polymer solutions were allowed to stand for 2 h at room temperature before filling in 700 μL omega-shaped plastic cuvettes (Anton Paar). The reported records are the average of the results of five individual measurements. The obtained electrophoretic mobility data were converted to zeta potentials based on the Smoluchowski equation [39].

3. Results and discussion

3.1. Rotational rheology of FLOPAAM 3630S

To examine the flow behavior of the polymer solutions studied, rotational tests were performed first. The flow curve recorded for the aqueous FLOPAAM 3630S polymer solution of 1.0 g/L concentration (Fig. 1) exemplifies the middle transition region of the three characteristic shear rate ranges of the Carreau model, which corresponds to the real (more accurately measurable) experimental region.

Based on the mathematical formula proposed by Carreau and Yasuda [13], the rheological material studied can be characterized by the viscosity function outlined in Fig. 1A. At low shear rates, the behavior of the Carreau fluid corresponding to the model is in line with a Newtonian fluid provided the viscosity is constant at zero-shear. In the intermediate or transient shear rate region, pseudo-plastic ($n < 1$), Newtonian ($n = 1$) and dilatant or otherwise shear-thickening ($n > 1$) behaviors are possible (equation (2)), depending on the degree of viscosity shear dependence determined by the Ostwald-de Waele power law appearance [40]. At high shear rates, the Carreau fluid is again characterized by a Newtonian viscosity of magnitude different from the zero-shear viscosity corresponding to the shear dependence (n) of the viscosity [10,41].

To facilitate the handling of experimental data from rheological measurements, a spreadsheet-based evaluation routine was developed for modelling the results of rotational rheological measurements with the Carreau-Yasuda model (grey continuous lines in Fig. 1. A). The spreadsheet routine can determine the infinite-shear viscosity (η_∞) and the zero-shear viscosity (η_0) and the value of the shear dependence (n) of the viscosity. To calculate the standard deviations of the above-mentioned parameters, the resampling "jackknife" procedure was applied using spreadsheet software [42]. In the case of the aqueous solution of FLOPAAM 3630S polymer at a concentration of 1.0 g/L (Fig. 1), the viscosity shear dependence was found to be $n = 0.380 \pm 0.002$ and it is characterized by $\eta_\infty = 1.94 \pm 0.10$ mPas and $\eta_0 = 412.5 \pm 1.7$ mPas zero-shear viscosity. These values changed to 0.912 ± 0.031, 4.31 ± 0.18 mPas and 35.5 ± 2.0 mPas, respectively, in the salt solution containing 270 g/L NaCl. Considering these results, one can conclude that such an extremely high salt concentration radically changes the rheological properties of the investigated polymer solution. The deviation in the rheological parameters may originate from the change in the structural coherence of the polymer chains and the corresponding gelation of the samples, as discussed later. Such a gelation may occur through hydrophobic intermolecular interactions. To further address this issue a systematic assessment of the flow properties was carried out as follows.

3.2. Effect of salinity on the flow properties of FLOPAAM 3630S

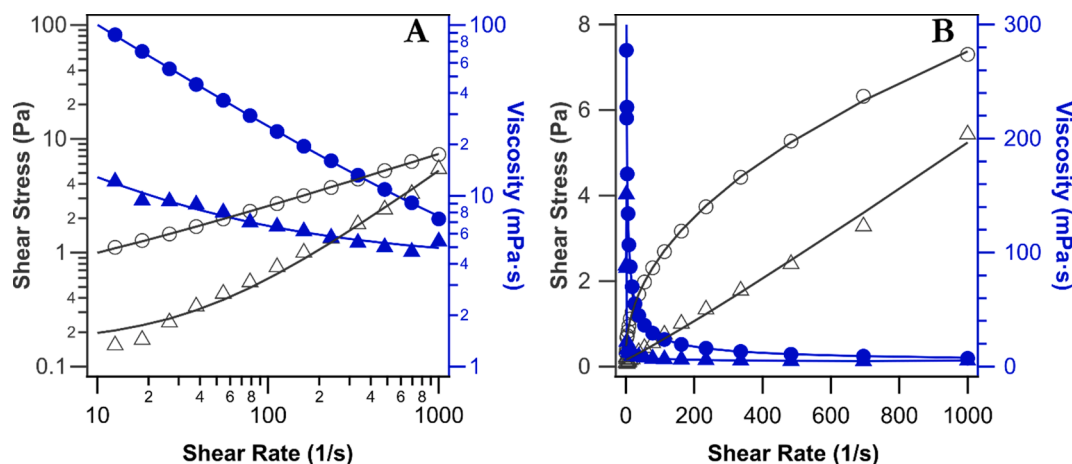The flow curves of the FLOPAAM 3630S were recorded in the NaCl

Fig. 1. Flow curves (shear stress versus shear rate) of 1.0 g/L FLOPAAM 3630S polymer dissolved in deionized water (empty circles) and 270 g/L NaCl solution (empty triangles) in log–log (A) and Bingham (B) representation. The filled symbols refer to the viscosity values at different shear rates. The viscosity and flow curves were fitted by the Carreau-Yasuda (A) and Herschel-Bulkley (B) equations and these fits are shown with solid lines.

concentration range of 0–270 g'/L. Although the Carreau-Yasuda relationship gives an excellent description of the flow properties of polymer solutions, the evaluation of a large amount of measurement data became necessary to describe the relationship between flow curves with less fitting parameters. Therefore, the Herschel-Bulkley model (equation (1)) was used, as this model is suitable for the investigation of both pseudoplastic and Newtonian fluids [33]. The recorded flow curves are shown in Fig. S1 (in SD), while the salinity-dependent yield point, flow index and apparent viscosity values are presented in Fig. 2.

The yield point (Fig. 2A) and apparent viscosity (Fig. 2C) values decreased (although the former one only until the highest salt level), and the flow indices (Fig. 2B) increased with increasing salt concentration (see also Table S1 for the data). This indicates that the intermolecular interactions between the polymer chains as well as the structural coherency weaken as the salinity increases in the samples. For instance, the decrease in the apparent viscosity reveals that the resistance of the polymer solution to flow is significantly reduced at high ionic strengths, which condition can be found also in the oil storage reservoir environment [25–27]. On the other hand, the trend in the flow index data points to pseudoplastic behavior up to about 10 g/L NaCl concentration and then reaching finally dilatant or shear-thickening condition indicated by the flow index around unity in the most concentrated salt solution. Based on this observation, it can be concluded that the flow behavior is mainly influenced by the change in the conformation, i.e., the solvation

state of the polymer, while the value of a flow index greater than one indicates the formation of a dispersive rheological object consisting of particles instead of a coherent colloidal system at elevated salinity. Concerning the increase of the yield point at the highest salt concentration, one can explain it with the findings of a recent report on the increase of electrostatic screening length in concentrated electrolytes [43]. Accordingly, it was observed that the Debye length in dilute electrolytes follows the expected trend, i.e., it decreases with the ionic strength, as predicted by the Debye-Hückel theory. However, at higher salt concentrations, when the Debye length becomes comparable to the size of molecules, this theory is no longer applicable. Instead, the effects of ion size and ion-ion correlations become significant in this regime, leading to an anomaly that deviates from classical approaches and for instance, influences the extent of inter and intramolecular hydrophobic interactions.

3.3. Oscillatory rheological measurements

To confirm the results obtained with the above analysis of the flow curves and for a more detailed understanding of the salinity-dependent rheological features of the polymer, oscillation measurements were performed. The results of the amplitude sweep tests performed without added salt and in the case of the highest salt concentration (270 g'/L) are shown in Fig. 3A.
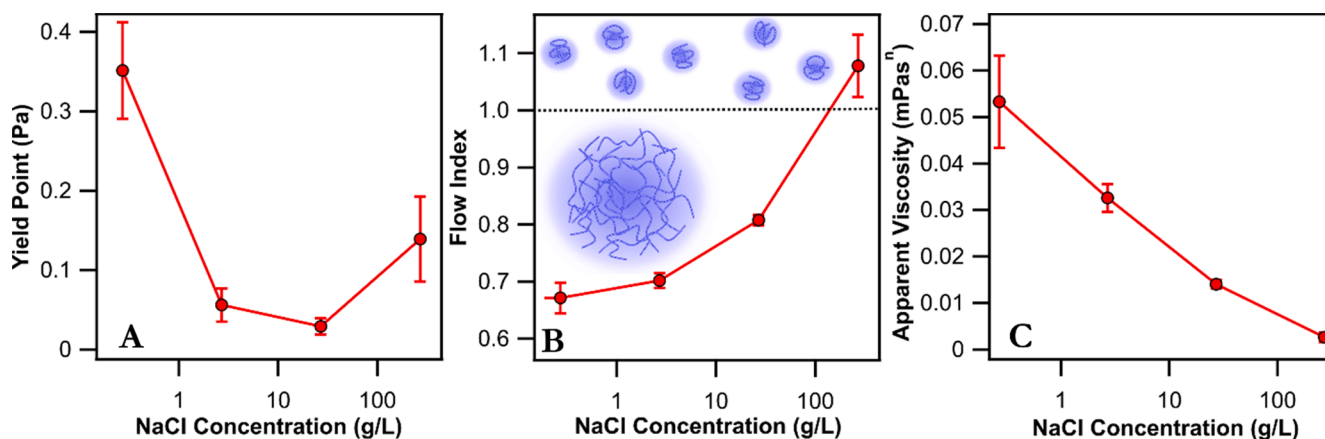

Fig. 2. Yield point (A), flow index (B) and apparent viscosity (C) of aqueous FLOPAAM 3630S polymer solutions at different NaCl concentrations determined by fitting the flow curves with the Herschel-Bulkley model (equation (1)). The continuous red lines are eye guides. (For interpretation of the references to colour in this figure legend, the reader is referred to the web version of this article.)
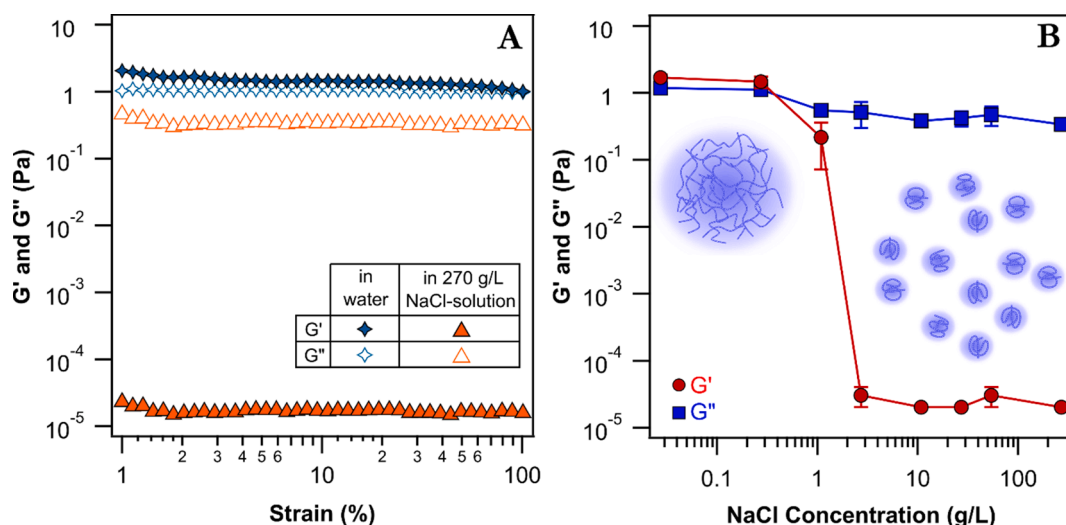
Fig. 3. Amplitude sweep test of FLOPAAM 3630S in water and 270 g/L salt solution at 1 g/L polymer concentration at 1–100 shear deformation and 10 Hz oscillation frequency (A). Storage (G'') and loss (G') moduli of the polymer solutions as a function of NaCl concentration (B). The polymer concentration was 1 g/L in all samples. The continuous lines serve to guide the eyes.

Typical viscoelastic behavior [44,45] was observed without adding NaCl. Accordingly, the storage modulus (G''), which is the measure of the sample's elastic behavior, was larger by several orders of magnitude than the values of the loss modulus (G'). Moreover, both moduli remain constant within the experimental error indicating that the linear viscoelastic region (LVE) covers the whole investigated deformation region. In contrast, at high salt concentrations, such a viscoelastic property disappears, and the values of storage and loss moduli are nearly the same. These results also shed light on the fact that the coherent (or gellike) structure of FLOPAAM3630 collapses upon salt addition.

To further quantify the coherent-incoherent structure transition, the mean values of the storage and loss moduli (Fig. 3B) were determined by amplitude sweep tests at various NaCl concentrations (Fig. S2 in SD). Although these parameters are nearly constant in the LVE range, the standard deviation of their average value can also be significant due to the unique properties of the samples and the measurement conditions. Accordingly, storage and loss moduli with a small standard error were determined at low and high salt concentrations, while the data were more uncertain in the coherent-incoherent transition regime, which was located between 0.5 and 2.0 g/L salt NaCl concentration. These results indicate that the rheological features of the FLOPAAM 3630S solutions

dramatically change from viscoelastic to simple viscous behavior in this intermediate salinity regime, which is relevant to salinities existing in oil reservoirs [46,47].

3.4. Structural assessment of FLOPAAM 3630S solutions

Light scattering techniques are powerful tools to investigate the structural features of polymer solutions [48–50]. However, finding the optimal conditions is challenging, since low polymer concentration leads to insufficient scattering signal, while multiple scattering events affect the measurements at high concentrations, e.g., in turbid samples [51]. The 3D cross-correlation technique [38] allowed to perform DLS experiments to assess the influence of the structural coherency of FLOPAAM 3630S on the correlation function at 1 g/L concentration, at which reliable DLS measurements could not be performed with conventional DLS instruments applying autocorrelation of the intensity of the scattered light. The intensity correlation functions obtained with the 3D cross-correlation technique for the FLOPAAM 3630S solutions at low (0.27 g/L) and high (270 g/L) NaCl concentrations are presented in Fig. 4.

The striking difference between the samples measured at low
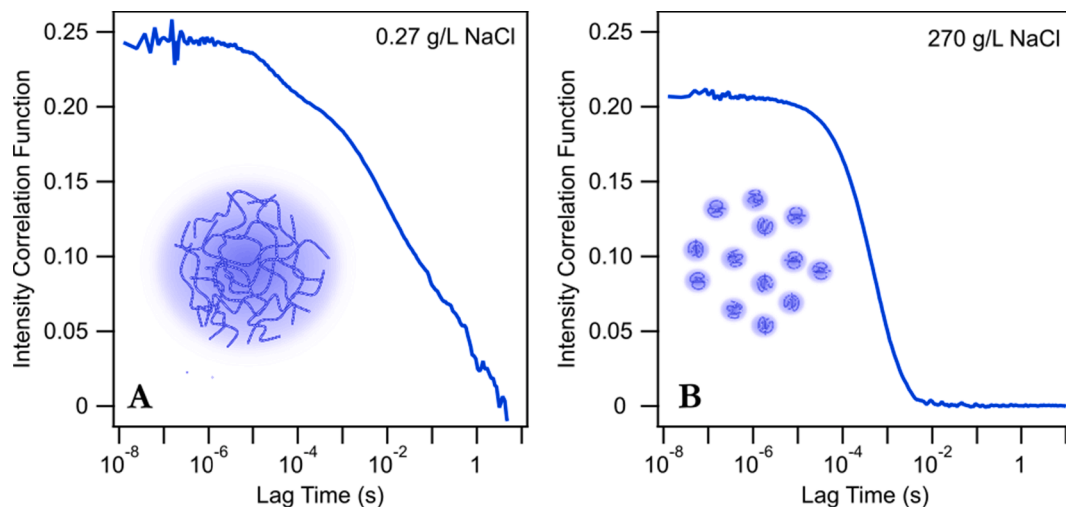
Fig. 4. 3D cross-correlation functions recorded with DLS using 1 g/L FLOPAAM 3630S polymer solutions in low (A, 0.27 g/L) and high (B, 270 g/L) salinity samples.

(Fig. 4A) and high (Fig. 4B) NaCl concentrations is the tendency in the decay of the correlation function. While it follows the expected exponential decay [52] at elevated salinity, non-ergodic behavior indicating the formation of polymeric gels, whose density fluctuations are partially frozen due to intermolecular interactions through hydrophobic forces [53] was observed at low NaCl concentration. These findings clearly support the conclusions of the rheological studies, i.e., structural coherency disappears at high salt levels and the forming macromolecular solution yields typical exponential decay of the correlation function due to the lack of strong interactions between the polymer chains and absence of gel formation.

3.5. Charge-structure relationship

The nature of the intermolecular interactions, i.e., the origin of the possible intermolecular forces, was studied in electrophoretic light scattering measurements. Accordingly, electrophoretic mobilities were determined at different ionic strengths and converted to zeta potentials [39]. The data are shown in Fig. 5A.

Based on the rheological and light scattering studies' findings, the salt concentration variation leads to the formation of two substantially different colloidal systems. At low salt concentrations, the coherent gel structure is characterized by high negative zeta potential, and then with increasing electrolyte concentration, the potential increases. Moreover, such a tendency can be divided into 2 regions since a sudden increase occurred around 0.5 g/L NaCl concentration, while a linear change in the data was found below and above this value, at which the start of the disappearance of coherent FLOPAAM 3630S structure was detected in the rheology measurements. This can be clearly noticed by the evaluation of the loss factor data (Fig. 5B) indicating the significant loss in the coherency in this NaCl concentration regime. In other words, the gel-like system is characterized by a low loss factor value, where δ is between 0° and 45, in contrast to higher salt conditions leading to the breakdown of the coherent structure. Here, the individual flow units are characterized by a larger loss factor indicating the appearance of a fluid state, where δ is between 45° and 90°.

It is evident from the above results that the electrophoretic behavior of the gel-like state is rather different from the macromolecular solutions, the magnitude of FLOPAAM 3630S charge is higher at low salinities. This is due to the dual effect of charge screening [54] and counterion condensations [55] into the polymeric structure. The latter one is especially favorable since a significant amount of sodium ions can be accommodated into the gel-like structure, while the outer part can be still highly charged. However, once individual polymer chains are present in the solutions, the charge screening effects are more pronounced giving rise to lower electrophoretic mobility and zeta potential values. Apart from such electrostatic interactions between salt constituents and FLOPAAM 3630S, intermolecular hydrophobic interactions may also occur, but their occurrence becomes rarer by increasing the salt level. Besides, intramolecular hydrophobic interactions are favorable once electrostatic forces are screened at intermediate salt levels, at which the classical Debye-Hückel theory is applicable to describe the electrostatic screening length [43], while its increase in concentrated electrolytes may lead to different conformation of the polymer chains and thus, to change in the physicochemical parameters of the solutions. However, no direct experimental evidence for the presence of hydrophobic interactions could be obtained from the present data.

4. Conclusions

Partially hydrolyzed acrylamides are widely used in EOR processes, while the salinity level of the reservoirs greatly influences the sweeping efficiency of such polymers. Based on the results of rheology, light scattering, and electrophoretic experiments, it was concluded that FLOPAAM 3630S forms gel-like structures in low salinity samples, while the coherency decreases by increasing the salt concentrations. The threshold value for the transition is between 0.5 and 2 g/L NaCl concentration. A striking change was observed in the zeta potentials, DLS correlation functions and rheological parameters (e.g., flow index, apparent viscosity, and loss factor) by increasing the salt level and the change was even more remarkable in the above salinity regime. Electrostatic salt constituent-polymer interactions play a crucial role in the formation and disappearance of the gel-like structure, while hydrophobic interactions may also occur at certain salinities. These findings provide important insights into the structure-rheology relation of an EOR polymer, which can be useful in the design of polymer flooding systems to be applied in oil reservoirs of various salt levels since the sweep efficiency can be predicted based on the rheological and structural features under different reservoir conditions.

CRediT authorship contribution statement

Zsófia Vargáné Árok: Data curation, Writing – original draft, Investigation. **Szilárd Sáringer:** Data curation, Visualization. **Dóra Takács:** Methodology. **Coline Bretz:** Investigation, Methodology. **Ádám Juhász:** Investigation, Writing – original draft,
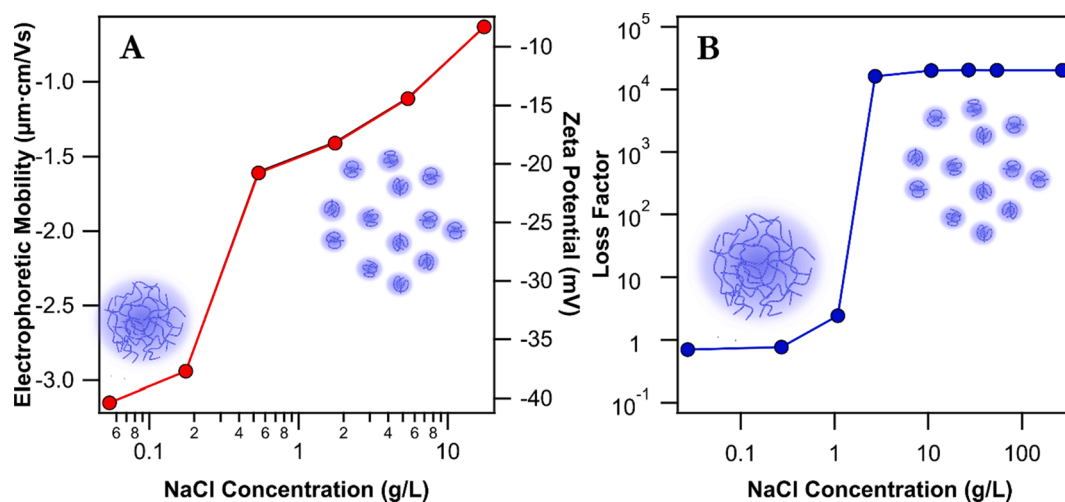
Fig. 5. The effect of salinity on the electrophoretic mobilities and zeta potentials of FLOPAAM 3630S polymer in NaCl solutions (A). Variation of the dimensionless loss factor (equation (5)) determined for FLOPAAM 3630S as a function of NaCl concentration (B). The polymer concentration was 1 g/L and the solid lines serve to guide the eyes.

Conceptualization. **Istvan Szilagyi:** Supervision, Writing – review & editing, Resources.

Declaration of Competing Interest

The authors declare that they have no known competing financial interests or personal relationships that could have appeared to influence the work reported in this paper.

Data availability

Data will be made available on request.

Acknowledgements

Appendix A. Supplementary material

Supplementary data to this article can be found online at https://doi.org/10.1016/j.molliq.2023.122192.

References

[1] W.H. Wang, Y. Xu, J.J. Ge, H.B. Guo, Q.H. Wu, Y. Mao, Phenolic resin gel suitable for medium-temperature and high-salinity reservoirs, J. Mol. Liq. 364 (2022), 119887.

[2] W.C. Wang, Y. Peng, Z.X. Chen, H.Q. Liu, J. Fan, Y.S. Liu, Synergistic effects of weak alkaline-surfactant-polymer and SiO$_2$ nanoparticles flooding on enhanced heavy oil recovery, Energy Fuels 36 (2022) 7402–7413.

[3] L.M. Corredor, M.M. Husein, B.B. Maini, A review of polymer nanohybrids for oil recovery, Adv. Colloid Interface Sci. 272 (2019), 102018.

[4] J.C. Liu, A. Almakimi, M.Z. Wei, B.J. Bai, I.A. Hussein, A comprehensive review of experimental evaluation methods and results of polymer micro/nanogels for enhanced oil recovery and reduced water production, Fuel 324 (2022), 124664.

[5] C. Temizel, M. Zhang, F. Biopharm, B. Jia, D. Putra, R. Moreno, B. Al-Otaibi, A. Alkouh, Next-generation gelling agents for improved displacement in enhanced oil recovery processes, SPE Kuwait Oil & Gas Show and Conference, OnePetro, Kuwait, 2017.

[6] G. Zhao, C. Dai, W. Li, Z. Yan, M. Zhao, Research on a temporary plugging agent based on polymer gel for reservoir acidification, J. Petrol. Explor. Prod. Technol. 6 (2016) 465–472.

[7] J.W. Liu, S.B. Wang, L. He, P. Hu, Y. Gao, Preparation and properties of nano-silica hybrid hydrophobic associated polyacrylamide for polymer flooding, J. Pet. Sci. Eng. 208 (2022), 109434.

[8] B. Wei, L. Romero-Zerón, D. Rodrigue, Oil displacement mechanisms of viscoelastic polymers in enhanced oil recovery (EOR): a review, J. Petrol. Explor. Prod. Technol. 4 (2014) 113–121.

[9] A.A. Olajire, Review of ASP EOR (alkaline surfactant polymer enhanced oil recovery) technology in the petroleum industry: Prospects and challenges, Energy 77 (2014) 963–982.

[10] J. Machale, S.K. Majumder, P. Ghosh, T.K. Sen, Development of a novel biosurfactant for enhanced oil recovery and its influence on the rheological properties of polymer, Fuel 257 (2019), 116067.

[11] S. Thomas, Enhanced oil recovery - An overview, Oil Gas Sci. Technol. 63 (2008) 9–19.

[12] B.B. Sandiford, Laboratory and field studies of water floods using polymer solutions to increase oil recoveries, J. Pet. Technol. 16 (1964) 917–922.

[13] E.E. Gomaa, J.H. Duerksen, P.T. Woo, Designing a steamflood pilot in the thick monarch sand of the midway-sunset field, J. Pet. Technol. 29 (1977) 1559–1568.

[14] J.P. Xu, Y.D. Yuan, Z. Feng, F. Liu, Z. Zhang, Molecular dynamics simulation of adsorption and diffusion of partially hydrolyzed polyacrylamide on kaolinite surface, J. Mol. Liq. 367 (2022), 120377.

[15] W.F. Pu, C. Shen, B. Wei, Y. Yang, Y.B. Li, A comprehensive review of polysaccharide biopolymers for enhanced oil recovery (EOR) from flask to field, J. Ind. Eng. Chem. 61 (2018) 1–11.

[16] S.D. Yuan, S.S. Liu, H. Zhang, S.L. Yuan, Understanding the role of host-guest interactions in enhancing oil recovery through beta cyclodextrin and adamantane modified copolymer, J. Mol. Liq. 369 (2023), 120841.

[17] A. Skauge, N. Zamani, J.G. Jacobsen, B.S. Shiran, B. Al-Shakry, T. Skauge, Polymer flow in porous media: Relevance to enhanced oil recovery, Colloid Interfac. 2 (2018) 27.

[18] S. Al-Hajri, S.M. Mahmood, H. Abdulelah, S. Akbari, An overview on polymer retention in porous media, Energies 11 (2018) 2751.

[19] B.Y. Jamaloei, Effect of wettability on immiscible viscous fingering: Part I, Mechanisms, Fuel 304 (2021), 120726.

[20] J.G. Lee, J.J. Huang, T. Babadagli, Dynamics of emulsion generation and stability during heavy oil displacement with chemicals and nanoparticles: Qualitative analysis using visual 2D data, Fuel 270 (2020) 23.

[21] S. Hill, P. Inst, Channeling in packed columns, Chem. Eng. Sci. 1 (1952) 247–253.

[22] P.G. Saffman, G.I. Taylor, The penetration of a fluid into a porous medium or Hele-Shaw cell containing a more viscous liquid, Proc. Royal Soc. London A 245 (1958) 312–329.

[23] K.S. Sorbie, A.Y. Al Ghafri, A. Skauge, E.J. Mackay, On the modelling of immiscible viscous fingering in two-phase flow in porous media, Transp. Porous Media 135 (2020) 331–359.

[24] D.W. Peaceman, H.H. Rachford Jr., Numerical calculation of multidimensional miscible displacement, Soc. Petroleum Eng. J. 2 (1962) 327–339.

[25] K. Liang, P.H. Han, Q.S. Chen, X. Su, Y.J. Feng, Comparative study on enhancing oil recovery under high temperature and high salinity: Polysaccharides versus synthetic polymer, ACS Omega 4 (2019) 10620–10628.

[26] M.A. Alzaabi, J.M. Leon, A. Skauge, S. Masalmeh, Analysis and simulation of polymer injectivity test in a high temperature high salinity carbonate reservoir, Polymers 13 (2021) 1765.

[27] X. Zhong, C.C. Li, Y.H. Li, H. Pu, Y.X. Zhou, J.X. Zhao, Enhanced oil recovery in high salinity and elevated temperature conditions with a zwitterionic surfactant and silica nanoparticles acting in synergy, Energy Fuels 34 (2020) 2893–2902.

[28] X.E. Li, Z. Xu, H.Y. Yin, Y.J. Feng, H.P. Quan, Comparative studies on enhanced oil recovery: Thermoviscosifying polymer versus polyacrylamide, Energy Fuels 31 (2017) 2479–2487.

[29] M.J. Data, J.M. Milanesio, R. Martini, M. Strumia, Synthesis techniques for polymers applied to enhanced oil recovery, MOJ Polym. Sci. 2 (2018) 17–20.

[30] K.S. Sorbie, Polymer-improved oil recovery, Springer, Dordrecht, New York, 1991.

[31] N. Gaillard, B. Giovannetti, T. Leblanc, A. Thomas, O. Braun, C. Favero, Selection of customized polymers to enhance oil recovery from high temperature reservoirs, SPE Latin American and Caribbean Petroleum, Engineering Conference (2015).

[32] J.K.M. William, S. Ponmani, R. Samuel, R. Nagarajan, J.S. Sangwai, Effect of CuO and ZnO nanofluids in xanthan gum on thermal, electrical and high pressure rheology of water-based drilling fluids, J. Pet. Sci. Eng. 117 (2014) 15–27.

[33] E. Magnon, E. Cayeux, Precise method to estimate the Herschel-Bulkley parameters from pipe rheometer measurements, Fluids 6 (2021) 157.

[34] M. Keentok, J.F. Milthorpe, E. Odonovan, On the shearing zone around rotating vanes in plastic liquids - theory and experiments, J. Non-Newton. Fluid Mech. 17 (1985) 23–35.

[35] J. Aho, S. Syrjala, On the measurement and modeling of viscosity of polymers at low temperatures, Polym. Test 27 (2008) 35–40.

[36] P.A. Hassan, S. Rana, G. Verma, Making sense of Brownian motion: Colloid characterization by dynamic light scattering, Langmuir 31 (2015) 3–12.

[37] J. Stetefeld, S.A. McKenna, T.R. Patel, Dynamic light scattering: a practical guide and applications in biomedical sciences, Biophys. Rev. 8 (2016) 409–427.

[38] I.D. Block, F. Scheffold, Modulated 3D cross-correlation light scattering: Improving turbid sample characterization, Rev. Sci. Instrum. 81 (2010), 123107.

[39] A.V. Delgado, F. Gonzalez-Caballero, R.J. Hunter, L.K. Koopal, J. Lyklema, Measurement and interpretation of electrokinetic phenomena, J. Colloid Interface Sci. 309 (2007) 194–224.

[40] S. Xun, J.H. Zhao, L.C. Zheng, X.H. Chen, X.X. Zhang, Flow and heat transfer of Ostwald-de Waele fluid over a variable thickness rotating disk with index decreasing, Int. J. Heat Mass Transf. 103 (2016) 1214–1224.

[41] N. Marx, L. Fernandez, F. Barcelo, H. Spikes, Shear thinning and hydrodynamic friction of viscosity modifier-containing oils. Part I: Shear thinning behaviour, Tribol. Lett. 66 (2018) 14.

[42] A. Juhasz, D. Ungor, K. Berta, L. Seres, E. Csapo, Spreadsheet-based nonlinear analysis of in vitro release properties of a model drug from colloidal carriers, J. Mol. Liq. 328 (2021), 115405.

[43] A.M. Smith, A.A. Lee, S. Perkin, The electrostatic screening length in concentrated electrolytes increases with concentration, J. Phys. Chem. Lett. 7 (2016) 2157–2163.

[44] E. Benigar, A.Z. Valant, I. Dogsa, S. Sretenovic, D. Stopar, A. Jamnik, M. Tomsic, Structure and dynamics of a model polymer mixture mimicking a levan-based bacterial biofilm of bacillus subtilis, Langmuir 32 (2016) 8182–8194.

[45] R.J.B. Motta, A.Z.F. Almeida, B.L.B. de Lima, R. Schneider, R.D. Balaban, J.S. van Duijneveldt, R.J. de Oliveira, Polyphosphates can stabilize but also aggregate colloids, Phys. Chem. Chem. Phys. 22 (2020) 15–19.

[46] M. Algharaib, A. Alajmi, R. Gharbi, Improving polymer flood performance in high salinity reservoirs, J. Pet. Sci. Eng. 115 (2014) 17–23.

[47] C. Duran-Valencia, B. Bai, H. Reyes, R. Fajardo-Lopez, F. Barragan-Aroche, S. Lopez-Ramirez, Development of enhanced nanocomposite preformed particle gels for conformance control in high-temperature and high-salinity oil reservoirs, Polym. J. 46 (2014) 277–284.

[48] W. Schärtl, Light scattering from polymer solutions and nanoparticle dispersions, Springer, Berlin, 2007.

[49] H. Matsuoka, Y. Ogura, H. Yamaoka, Effect of counterion species on the dynamics of polystyrenesulfonate in aqueous solution as studied by dynamic light scattering, J. Chem. Phys. 109 (1998) 6125–6132.

[50] M. Usuelli, Y.P. Cao, M. Bagnani, S. Handschin, G. Nystrom, R. Mezzenga, Probing the structure of filamentous nonergodic gels by dynamic light scattering, Macromolecules 53 (2020) 5950–5956.

[51] M.I. Mishchenko, L.D. Travis, A.A. Lacis, Scattering, absorption, and emission of light by small particles, University Press, Cambridge, 2002.

[52] P.N. Pusey, Dynamic light scattering, in: P. Lindner, T. Zemb (Eds.), Neutrons, X-Rays and Light, Elsevier Science B.V, Amsterdam, 2002, pp. 203–220.

[53] P.N. Pusey, Dynamic light-scattering by nonergodic media, Macromol. Symp. 79 (1994) 17–30.

[54] M. Borkovec, G.J.M. Koper, C. Piguet, Ion binding to polyelectrolytes, Curr. Opin. Colloid Interface Sci. 11 (2006) 280–289.

[55] G.S. Manning, Limiting laws and counterion condensation in polyelectrolyte solutions 1. Colligative properties, J. Chem. Phys. 51 (1969) 924–933.